2025 APPLICATIONS OF MATHEMATICS 22 pp
Online first

QUALITATIVE ANALYSIS OF HAART EFFECTS ON HIV AND SARS-COV-2 COINFECTION MODEL

João Paulo Simões Maurício de Carvalho

Received December 16, 2024. Published online July 11, 2025.

Abstract. HIV is known for causing the destruction of the immune system by affecting different types of cells, while SARS-CoV-2 is an extremely contagious virus that leads to the development of COVID-19. Understanding how these two viruses interact in coinfected individuals is essential, especially in populations under antiretroviral treatment. In this study, we develop and analyze a novel mathematical model capturing the coinfection dynamics of HIV and SARS-CoV-2 under the influence of highly active antiretroviral therapy (HAART). In contrast to previous models, our formulation includes the effect of HAART on both infections and derives the basic reproduction numbers for each virus. We prove that transcritical bifurcations occur when the basic reproduction numbers cross the threshold value of 1, and we establish the conditions for stability of the disease-free equilibria. Numerical simulations show that HAART, although designed to control HIV, also reduces SARS-CoV-2 proliferation in coinfected hosts, which, as far as we know, has not been fully addressed in previous models in the literature. These findings reveal a potentially beneficial indirect effect of antiretroviral therapy on SARS-CoV-2 dynamics, offering new theoretical insights into the control of viral coinfections.

Keywords: bifurcation analysis; basic reproduction number; HAART; coinfection

MSC 2020: 34C11, 34C23, 34C60, 37N25, 37N30, 65Z05, 92B05

1. Introduction

The first official case of CoViD-19 in China emerged in December 2019 and was linked to the Huanan seafood market, in Wuhan [9]. Since then SARS-CoV-2 has reached 219 countries and territories having infected more than 775 million people, thus becoming a global pandemic and causing more than 7 million deaths worldwide [24]. The most frequently noticed symptoms in infected people are fever, cough and respiratory disorders [19], [23]. The most affected people are elderly and adults

Open access funding provided by FCT—FCCN (b-on).

DOI: 10.21136/AM.2025.0280-24

over 60 years old and/or those with comorbidities, such as obesity, diabetes, oncological diseases, heart problems, among others [2], [13], [17].

HIV continues to be a global health challenge, with 42.3 million deaths to date and ongoing transmission around the world. According to the World Health Organization (WHO), at the end of 2023, around 39.9 million people were living with HIV, of whom approximately 75% have access to antiretroviral treatment [3] and 65% of them in the WHO African Region. That same year, 1.3 million new infections were recorded and 630 000 people died from HIV-related causes. Although there is no cure for HIV, access to prevention, diagnosis and treatment helps people manage the virus as a long-term disease. World health organizations are working to end the HIV epidemic by 2030 [25].

Coinfection by HIV and SARS-CoV-2 raises a significant public health concern, since both diseases affect the immune system in distinct and complex ways. HIV progressively weakens the body's immune defenses, while SARS-CoV-2 can trigger severe and potentially dysregulated immune responses. In seropositive individuals, the interaction between these two viruses can aggravate the clinical progression of COVID-19 [8], increase susceptibility to opportunistic infections and affect the effectiveness of antiviral treatments.

From a mathematical perspective, studying the dynamics of this coinfection is essential to understanding how the two viruses interact and impact the health outcomes of patients. Mathematical models allow us to explore the progression of infection in specific populations, predict outbreak scenarios and assess the impact of different interventions, such as combination therapies and vaccination campaigns [5], [15]. For individuals living with HIV and contracting COVID-19, these models are particularly valuable since they help identify factors that can exacerbate the clinical picture and assist in the design of more effective treatment strategies, both from an immunological and epidemiological point of view [8], [14].

State of the art.[1] In 2022, Mekonena and Obsu [12] analyzed a model for TB-COVID-19 coinfection, compartmentalizing the population into seven classes. The authors computed the basic reproduction numbers for each disease, showing that the disease-free and endemic equilibria remain stable (or unstable) if these numbers are lower (or higher) than one. The sensitivity analysis suggested that reducing contact rates and increasing the speed of transitions from latent to infected can reduce the spread of both diseases.

In 2022, Batu et al. [4] developed a mathematical model to study the impact of intervention strategies and identify mortality risk factors in seropositive people infected with COVID-19. Numerical simulations, based on data from Ethiopia, re-

[1] Other relevant models can be found in the literature; only key examples are presented here.

vealed that vaccination against COVID-19 and increased treatment rates reduce cases of coinfection and the risk of mortality for HIV-infected individuals, underlining the importance of vaccination programs and medical interventions.

In 2024, Vemparala et al. [22] studied a model based on HIV-1 control and remission through mathematical modeling. The authors explored the mechanisms behind natural and post-treatment control of HIV-1, assessed the potential causes of loss of control and quantified the effects of intervention. Their work highlights both the progress achieved in the optimization of the intervention and the ongoing challenges in applying these results in practical contexts.

During the same year, Chen et al. [6] studied an HIV virus-cell model with intracellular delays, focusing on the interactions between wild-type and drug-resistant HIV strains. The authors set stability criteria based on the basic reproduction number and analyzed Hopf bifurcations, finding that interactions between two strains lead to more complex dynamics, including higher viral loads and potential instability. They found that drug resistance influences the wild-type strain's survival, with an impact on HIV transmission.

Novelty and contribution. Although previous works have examined the dynamics of coinfection, none of them provide a rigorous mathematical analysis of HIV and SARS-CoV-2 coinfection under antiretroviral treatment. Furthermore, contributions such as [6] and [22] focus mainly on HIV dynamics or resistance within HIV strains, without addressing the added complexity of a coinfection system. In contrast, our work proposes and analyses a novel mathematical model that includes both HIV and SARS-CoV-2 dynamics under the effect of HAART. We derive analytical expressions for the basic reproduction numbers, study transcritical bifurcations in each submodel and determine the conditions for the stability of the disease-free equilibrium of the complete system. This provides theoretical evidence of a positive indirect effect of HAART on coinfection control, which to our knowledge has not been fully addressed in previous modeling literature.

Article structure. We describe the model and the population dynamics in Section 2. In Section 3 we prove the positivity and boundedness of the solutions of the coinfection model, analyze the equilibria of the HIV and SARS-CoV-2 submodels and their basic reproduction numbers. We also present our main results, followed by their proofs in Sections 5 and 6. In Section 4 we carry out a sensitivity analysis of the parameters that constitute the basic reproduction numbers for each submodel. We perform several numerical simulations in Section 7, and in Section 8 we present our conclusions and discuss potential future work.

With this work we aim to understand how HAART therapy affects the dynamics of viral load and cells infected with SARS-CoV-2. For this purpose, we will first

perform an analytical study of the model before exploring the interaction of both viruses in the presence of HAART through numerical simulations.

2. Model formulation

The model we propose is subdivided into four cell populations (cell population P_C):

T: number of healthy/target cells susceptible to infection;
I_H: number of cells that are currently infected by HIV;
I_S: number of cells that are currently infected by SARS-CoV-2;
C: number of cells that are currently coinfected by HIV and SARS-CoV-2,

and two classes of virus (virus population P_V):

V_H: HIV viral load;
V_S: SARS-CoV-2 viral load.

Let

$$\dot{X} = \mathcal{F}(X) \Leftrightarrow \begin{cases} \dot{T} = \lambda - k_1(1-\varepsilon_{RT})TV_H - k_2TV_S - \mu T, \\ \dot{I}_H = k_1(1-\varepsilon_{RT})TV_H - k_2I_HV_S - \mu I_H, \\ \dot{I}_S = k_2TV_S - k_1(1-\varepsilon_{RT})I_SV_H - \mu I_S, \\ \dot{V}_H = n_H(1-\varepsilon_P)\mu I_H - \sigma_H V_H, \\ \dot{V}_S = n_S\mu I_S - \sigma_S V_S, \\ \dot{C} = k_1(1-\varepsilon_{RT})I_SV_H + k_2I_HV_S - \mu C \end{cases} \tag{1}$$

be the nonlinear system of ODE that modulates the interaction between cells and virus, where

$$X(t) = (T(t), I_H(t), I_S(t), V_H(t), V_S(t), C(t)),$$

$$\dot{X} = (\dot{T}, \dot{I}_H, \dot{I}_S, \dot{V}_H, \dot{V}_S, \dot{C}) = \left(\frac{\mathrm{d}T}{\mathrm{d}t}, \frac{\mathrm{d}I_H}{\mathrm{d}t}, \frac{\mathrm{d}I_S}{\mathrm{d}t}, \frac{\mathrm{d}V_H}{\mathrm{d}t}, \frac{\mathrm{d}V_S}{\mathrm{d}t}, \frac{\mathrm{d}C}{\mathrm{d}t}\right),$$

and

$$\Psi = \{(\lambda, k_1, k_2, \mu, \varepsilon_{RT}, \varepsilon_P, n_H, n_S, \sigma_H, \sigma_S) \in (\mathbb{R}^+)^{10}\}$$

is the set of parameters of (1). The vector field associated to (1) will be called $\mathcal{F}$ and the associated flow is

$$\psi(t, (T_0, I_{H0}, I_{S0}, V_{H0}, V_{S0}, C_0)), \quad t \in \mathbb{R}_0^+, \quad (T_0, I_{H0}, I_{S0}, V_{H0}, V_{S0}, C_0) \in (\mathbb{R}_0^+)^6.$$

Model assumptions. The model was developed specifically for this study. It extends classical virus-host interaction models by incorporating the dynamics of HIV

and SARS-CoV-2 coinfection under the effect of HAART. The main assumptions reflect established biological knowledge: HAART reduces HIV replication and promotes immune recovery, which in turn may potentially limit the availability of susceptible cells for SARS-CoV-2 infection.

Dynamics and interpretation of the constants. The constant production rate of healthy T cells is given by λ. Healthy T cells are infected by HIV and SARS-CoV-2 at a rate k_1 and k_2, respectively. The parameter $0 \leqslant \varepsilon_{RT} \leqslant 1$ represents the efficacy of reverse transcriptase inhibitors (RTI), reaching 100% effectiveness when $\varepsilon_{RT} = 1$. Similarly, $0 \leqslant \varepsilon_P \leqslant 1$ denotes the efficacy of protease inhibitors (PI), with $\varepsilon_P = 1$ indicating full effectiveness. HIV and SARS-CoV-2 are produced by infected cells with the bursting size n_H and n_S, respectively. The natural death rates of T, I_H, I_S and C cells are given by μ_T, μ_H, μ_S and μ_C, respectively. However, for convenience in algebraic calculations, we will assume an equal natural death rate μ for all cells. The death rate of HIV is given by σ_H. The viral load of SARS-CoV-2 dies at a rate σ_S. The description and value of these parameters can be found in Table 2 and the dynamics of the cell and virus populations are given by

$$P_C(t) = T(t) + I_H(t) + I_S(t) + C(t) \tag{2}$$

and

$$P_V(t) = V_H(t) + V_S(t), \tag{3}$$

respectively. Figure 1 illustrates a diagram depicting the interactions among $P_C(t)$ under the HIV and SARS-CoV-2 viral loads. Moreover, the dynamics of all classes of (1) are given by

$$N(t) = P_C(t) + P_V(t) = T(t) + I_H(t) + I_S(t) + V_H(t) + V_S(t) + C(t).$$

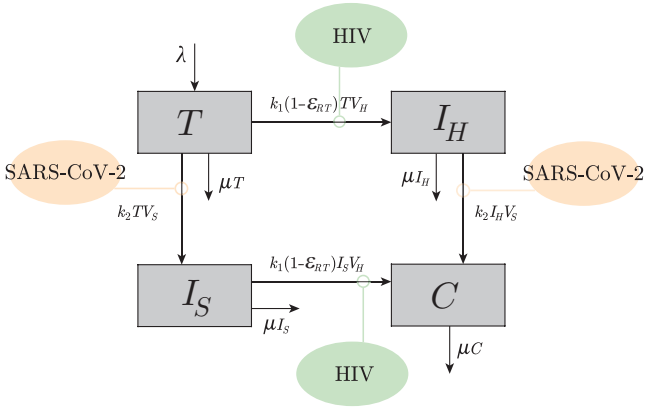

Figure 1. Diagram of the interactions between T, I_H, I_S and C cells of system (1) under the influence of the viral loads HIV and SARS-CoV-2.

3. Properties of the model and main results

In this section we prove that all solutions of system (1) are positive and bounded. Moreover, we analyze two submodels, HIV and SARS-CoV-2, derived from system (1).

Positivity and boundedness of solutions.

Theorem 1. *The solutions for T, I_H, I_S, V_H, V_S and C of model* (1) *are nonnegative and remain bounded for all $t \geqslant 0$ within the biologically feasible region defined by the set*

$$\Omega = \left\{ (T, I_H, I_S, V_H, V_S, C) \in (\mathbb{R}_0^+)^6 \colon\ 0 \leqslant P_C \leqslant \frac{\lambda}{\mu}, \right.$$
$$\left. 0 \leqslant P_V \leqslant \frac{n_H(1-\varepsilon_P)\mu I_H^{\max} + n_S \mu I_S^{\max}}{\sigma} \right\}.$$

P r o o f. For the active population and virus of system (1) we have

$$\begin{aligned}
\frac{\mathrm{d}T}{\mathrm{d}t}\Big|_{T=0} &= \lambda > 0,\\
\frac{\mathrm{d}I_H}{\mathrm{d}t}\Big|_{I_H=0} &= k_1(1-\varepsilon_{RT})TV_H \geqslant 0,\\
\frac{\mathrm{d}I_S}{\mathrm{d}t}\Big|_{I_S=0} &= k_2 T V_S \geqslant 0,\\
\frac{\mathrm{d}V_H}{\mathrm{d}t}\Big|_{V_H=0} &= n_H(1-\varepsilon_P)\mu I_H \geqslant 0,\\
\frac{\mathrm{d}V_S}{\mathrm{d}t}\Big|_{V_S=0} &= n_S \mu I_S \geqslant 0,\\
\frac{\mathrm{d}C}{\mathrm{d}t}\Big|_{C=0} &= k_1(1-\varepsilon_{RT})I_S V_H + k_2 I_H V_S \geqslant 0.
\end{aligned}$$

This demonstrates that $(\mathbb{R}_0^+)^6$ is positively invariant. Now, if we prove that P_C and P_V are both bounded, then N is bounded. Consequently, each population and virus is bounded. Hence, from (2) we have:

$$\begin{aligned}
\dot{P_C} &= \dot{T} + \dot{I}_H + \dot{I}_S + \dot{C}\\
&= \lambda - k_1(1-\varepsilon_{RT})TV_H - k_2 T V_S - \mu T\\
&\quad + k_1(1-\varepsilon_{RT})TV_H - k_2 I_H V_S - \mu I_H\\
&\quad + k_2 T V_S - k_1(1-\varepsilon_{RT})I_S V_H - \mu I_S\\
&\quad + k_1(1-\varepsilon_{RT})I_S V_H + k_2 I_H V_S - \mu C
\end{aligned}$$

$$= \lambda - \mu(T + I_H + I_S + C)$$
$$= \lambda - \mu P_C.$$

Using the classical differential version of Gronwall's Lemma, we have

$$P_C(t) \leqslant P_{C0}\mathrm{e}^{-\mu t} - \frac{\lambda}{\mu}(\mathrm{e}^{-\mu t} - 1),$$

from where we conclude that

$$0 \leqslant \lim_{t\to\infty} P_C(t) \leqslant \lim_{t\to\infty}\left[P_{C0}\mathrm{e}^{-\mu t} - \frac{\lambda}{\mu}(\mathrm{e}^{-\mu t} - 1)\right] = \frac{\lambda}{\mu}.$$

Then T, I_H, I_S and C are bounded. From (3) we write P_V as:

$$\dot{P_V} = \dot{V}_H + \dot{V}_S = n_H(1-\varepsilon_P)\mu I_H - \sigma_H V_H + n_S\mu I_S - \sigma_S V_S.$$

Let us consider $\sigma_H = \sigma_S = \sigma$. Since I_H and I_S are bounded, then we use $I_H^{\max}$ and $I_S^{\max}$ for the maximum values. Hence, rewriting $\dot{P}_V$ we get

$$\begin{aligned}\dot{P_V} &= n_H(1-\varepsilon_P)\mu I_H^{\max} + n_S\mu I_S^{\max} - \sigma(V_H + V_S)\\ &= n_H(1-\varepsilon_P)\mu I_H^{\max} + n_S\mu I_S^{\max} - \sigma P_V,\end{aligned}$$

and making use of the classical differential version of Gronwall's Lemma, we get

$$0 \leqslant \lim_{t\to\infty} P_V(t) \leqslant \lim_{t\to\infty}\left[P_{V0}\mathrm{e}^{-\sigma t} - \frac{n_H(1-\varepsilon_P)\mu I_H^{\max} + n_S\mu I_S^{\max}}{\sigma}(\mathrm{e}^{-\sigma t} - 1)\right]$$

$$\Leftrightarrow 0 \leqslant \lim_{t\to\infty} P_V(t) \leqslant \frac{n_H(1-\varepsilon_P)\mu I_H^{\max} + n_S\mu I_S^{\max}}{\sigma}.$$

Then, V_H and V_S are bounded and the Theorem is proved. □

We compute the basic reproduction number of HIV and SARS-CoV-2 submodels.

Submodel analysis. In the context of this work, the basic reproduction number $\mathcal{R}_0$ is the number of secondary infections due to a single infected cell in a susceptible healthy cell population [21].

HIV submodel. There is no SARS-CoV-2, imposing $I_S = V_S = C = 0$:

$$\dot{x}_{\mathrm{hiv}} = f(x_{\mathrm{hiv}}) \Leftrightarrow \begin{cases}\dot{T} = \lambda - k_1(1-\varepsilon_{RT})TV_H - \mu T,\\ \dot{I}_H = k_1(1-\varepsilon_{RT})TV_H - \mu I_H,\\ \dot{V}_H = n_H(1-\varepsilon_P)\mu I_H - \sigma_H V_H\end{cases} \tag{4}$$

with $x_{\mathrm{hiv}} = (T, I_H, V_H) \in (\mathbb{R}_0^+)^3$.

SARS-CoV-2 submodel. There is no HIV, imposing $I_H = V_H = C = 0$:

$$\dot{x}_{\text{sars}} = f(x_{\text{sars}}) \Leftrightarrow \begin{cases} \dot{T} = \lambda - k_2 T V_S - \mu T, \\ \dot{I}_S = k_2 T V_S - \mu I_S, \\ \dot{V}_S = n_S \mu I_S - \sigma_S V_S \end{cases} \tag{5}$$

with $x_{\text{sars}} = (T, I_S, V_S) \in (\mathbb{R}_0^+)^3$. The vector field associated to (4) and (5) is denoted by $f(x_{\text{hiv}})$ and $f(x_{\text{sars}})$, respectively. Their flows are

$$\psi_{\text{hiv}}(t, (T_0, I_{H0}, V_{H0})), \quad t \in \mathbb{R}_0^+, \quad (T_0, I_{H0}, V_{H0}) \in (\mathbb{R}_0^+)^3$$

and

$$\psi_{\text{sars}}(t, (T_0, I_{S0}, V_{S0})), \quad t \in \mathbb{R}_0^+, \quad (T_0, I_{S0}, V_{S0}) \in (\mathbb{R}_0^+)^3,$$

respectively. Using the same method as in [21] we compute the basic reproduction number for (4) and (5). The disease-free equilibrium of system (4) is given by:

$$E_{\text{hiv}} = (T_{\text{hiv}}, I_{H\,\text{hiv}}, V_{H\,\text{hiv}}) = \left(\frac{\lambda}{\mu}, 0, 0\right).$$

The matrix F_{hiv} is the matrix where the entries represent the new HIV infections and the matrix V_{hiv} represents the remaining terms:

$$F_{\text{hiv}} = \begin{pmatrix} 0 & k_1(1-\varepsilon_{RT})T_{\text{hiv}} \\ 0 & 0 \end{pmatrix}, \quad V_{\text{hiv}} = \begin{pmatrix} \mu & 0 \\ -n_H(1-\varepsilon_P)\mu & \sigma_H \end{pmatrix}.$$

Then through [21], Lemma 1, the basic reproduction number associated to model (4) is given by

$$\mathcal{R}_{\text{hiv}} = \varrho(F_{\text{hiv}} V_{\text{hiv}}^{-1}) = \frac{k_1 n_H (1-\varepsilon_{RT})(1-\varepsilon_P)\lambda}{\mu \sigma_H}, \tag{6}$$

where ϱ indicates the spectral radius of $F_{\text{hiv}} V_{\text{hiv}}^{-1}$. The disease-free equilibrium of system (5) is given by

$$E_{\text{sars}} = (T_{\text{sars}}, I_{S\,\text{sars}}, V_{S\,\text{sars}}) = \left(\frac{\lambda}{\mu}, 0, 0\right).$$

The matrix F_{sars} is the matrix, where the entries represent the new SARS-CoV-2 infections and the matrix V_{sars} represents the remaining terms:

$$F_{\text{sars}} = \begin{pmatrix} 0 & k_2 T_{\text{sars}} \\ 0 & 0 \end{pmatrix}, \quad V_{\text{sars}} = \begin{pmatrix} \mu & 0 \\ -n_S \mu & \sigma_S \end{pmatrix}.$$

Therefore, through [21], Lemma 1, the basic reproduction number associated to model (5) is given by

$$\mathcal{R}_{\text{sars}} = \varrho(F_{\text{sars}} V_{\text{sars}}^{-1}) = \frac{k_2 n_S \lambda}{\mu \sigma_S}, \tag{7}$$

where ϱ indicates the spectral radius of $F_{\text{sars}} V_{\text{sars}}^{-1}$.

Main results. Let E^e_{hiv} and E^e_{sars} be the endemic equilibria of (4) and (5), respectively. We set the following results:

Theorem 2. *Let $\mathcal{R}_{\text{hiv}}$ and $\mathcal{R}_{\text{sars}}$ be the basic reproduction numbers of HIV and SARS-CoV-2 submodels, respectively. Therefore,*

(i) *E^e_{hiv} undergoes a transcritical bifurcation at $\mathcal{R}_{\text{hiv}} = 1$, and lies in the interior of the first octant if $\mathcal{R}_{\text{hiv}} > 1$;*
(ii) *E^e_{sars} undergoes a transcritical bifurcation at $\mathcal{R}_{\text{sars}} = 1$, and lies in the interior of the first octant if $\mathcal{R}_{\text{sars}} > 1$.*

Now, let $\mathcal{R}_0$ be the basic reproduction number and E_{DFE} be the disease-free equilibrium of the full model (1).

Theorem 3. *The basic reproduction number of model* (1) *is equal to $\mathcal{R}_0 = \max\{\mathcal{R}_{\text{hiv}}, \mathcal{R}_{\text{sars}}\}$. Moreover, the disease-free equilibrium point E_{DFE} is locally asymptotically stable when $\mathcal{R}_0 < 1$. Otherwise it is unstable.*

In Section 5 and Section 6 we present the proof of Theorem 2 and Theorem 3, respectively.

4. Sensitivity analysis of $\mathcal{R}_{\text{hiv}}$ and $\mathcal{R}_{\text{sars}}$

Sensitivity indices are used to evaluate how a variable varies in response to changes in a given parameter. These indices represent the ratio between the relative change in the variable and the relative change in the parameter. In the case where the variable v is a differentiable function of the parameter p, the sensitivity index can be computed using partial derivatives as follows [7], [10]:

$$\varphi_p^v = \frac{\partial v}{\partial p} \times \frac{p}{v}.$$

When considering the specific case of the basic reproduction number $\mathcal{R}$, we have:

$$\varphi_p^{\mathcal{R}} = \frac{\partial \mathcal{R}}{\partial p} \times \frac{p}{\mathcal{R}}.$$

We compute the signs of the sensitivity indices related to $\mathcal{R}_{\text{hiv}}$ and $\mathcal{R}_{\text{sars}}$ and we present them in Table 1.

Index	Sensitivity index sign ($\mathcal{R}_{\text{hiv}}$)	Index	Sensitivity index sign ($\mathcal{R}_{\text{sars}}$)
$\varphi_{k_1}^{\mathcal{R}_{\text{hiv}}}$	$+1$	$\varphi_{k_2}^{\mathcal{R}_{\text{sars}}}$	$+1$
$\varphi_{n_H}^{\mathcal{R}_{\text{hiv}}}$	$+1$	$\varphi_{n_S}^{\mathcal{R}_{\text{sars}}}$	$+1$
$\varphi_{\varepsilon_{RT}}^{\mathcal{R}_{\text{hiv}}}$	$-\dfrac{\varepsilon_{RT}}{1-\varepsilon_{RT}} < 0$		
$\varphi_{\varepsilon_P}^{\mathcal{R}_{\text{hiv}}}$	$-\dfrac{\varepsilon_P}{1-\varepsilon_P} < 0$		
$\varphi_{\lambda}^{\mathcal{R}_{\text{hiv}}}$	$+1$	$\varphi_{\lambda}^{\mathcal{R}_{\text{sars}}}$	$+1$
$\varphi_{\mu}^{\mathcal{R}_{\text{hiv}}}$	-1	$\varphi_{\mu}^{\mathcal{R}_{\text{sars}}}$	-1
$\varphi_{\sigma_H}^{\mathcal{R}_{\text{hiv}}}$	-1	$\varphi_{\sigma_S}^{\mathcal{R}_{\text{sars}}}$	-1

Table 1. Sensitivity indices for the parameters of $\mathcal{R}_{\text{hiv}}$ and $\mathcal{R}_{\text{sars}}$.

The transmission rates k_1 and k_2 contribute to the increase in the basic reproduction number of HIV and SARS-CoV-2, respectively. The parameters n_H, n_S and λ have the same effect on the respective basic reproduction numbers. On the other hand, the parameters relating to treatment and mortality rates of infected cells and viruses have the opposite effect, i.e., increasing the values of these parameters has a retarding effect on the basic reproduction number of the respective viruses.

5. Proof of Theorem 2

With respect to the HIV submodel (4), through Theorem 2 of [21], we obtain the following lemma:

Lemma 1. *If $\mathcal{R}_{\text{hiv}} < 1$, then the disease-free equilibrium point E_{hiv} of (4) is locally asymptotically stable. Otherwise it is unstable.*

Proof. Let

$$\mathcal{J}_{\text{hiv}} = \begin{pmatrix} -k_1(1-\varepsilon_{RT})V_{H\,\text{hiv}} - \mu & 0 & -k_1(1-\varepsilon_{RT})T_{\text{hiv}} \\ k_1(1-\varepsilon_{RT})V_{H\,\text{hiv}} & -\mu & k_1(1-\varepsilon_{RT})T_{\text{hiv}} \\ 0 & n_H(1-\varepsilon_P)\mu & -\sigma_H \end{pmatrix} \tag{8}$$

$$= \begin{pmatrix} -\mu & 0 & -\dfrac{k_1(1-\varepsilon_{RT})\lambda}{\mu} \\ 0 & -\mu & \dfrac{k_1(1-\varepsilon_{RT})\lambda}{\mu} \\ 0 & n_H(1-\varepsilon_P)\mu & -\sigma_H \end{pmatrix}$$

be the matrix of linearization of model (4) around E_{hiv}. Then the associated eigenvalues are:

$$\varphi_1 = -\mu,$$

$$\varphi_2 = \frac{-(\sigma_H + \mu) + \sqrt{4n_H\lambda(1-\varepsilon_{RT})(1-\varepsilon_P)k_1 + (\mu - \sigma_H)^2}}{2},$$

$$\varphi_3 = \frac{-(\sigma_H + \mu) - \sqrt{4n_H\lambda(1-\varepsilon_{RT})(1-\varepsilon_P)k_1 + (\mu - \sigma_H)^2}}{2}.$$

It is trivial to see that the eigenvalues φ_1 and φ_3 have negative real part. Regarding the eigenvalue φ_2, it has negative real part if

$$\begin{aligned}
&-(\sigma_H + \mu) + \sqrt{4n_H\lambda(1-\varepsilon_{RT})(1-\varepsilon_P)k_1 + (\mu - \sigma_H)^2} < 0 \\
&\quad \Leftrightarrow 4n_H\lambda(1-\varepsilon_{RT})(1-\varepsilon_P)k_1 + (\mu - \sigma_H)^2 < (\sigma_H + \mu)^2 \\
&\quad \Leftrightarrow k_1 n_H(1-\varepsilon_{RT})(1-\varepsilon_P)\lambda < \mu\sigma_H \\
&\quad \overset{(6)}{\Leftrightarrow} \mathcal{R}_{\text{hiv}} < 1.
\end{aligned}$$

Hence, $\varphi_2 < 0$ and all eigenvalues have negative real part if $\mathcal{R}_{\text{hiv}} < 1$. This proves Lemma 1. □

Now, computing E^e_{hiv}, we get

$$E^e_{\text{hiv}} = (T^e_{\text{hiv}}, {I_H}^e_{\text{hiv}}, {V_H}^e_{\text{hiv}}),$$

where

$$\begin{aligned}
T^e_{\text{hiv}} &= \frac{\sigma_H}{n_H k_1(1-\varepsilon_{RT})(1-\varepsilon_P)}, \\
{I_H}^e_{\text{hiv}} &= \frac{n_H k_1\lambda(1-\varepsilon_{RT})(1-\varepsilon_P) - \mu\sigma_H}{n_H\mu k_1(1-\varepsilon_{RT})(1-\varepsilon_P)}, \\
{V_H}^e_{\text{hiv}} &= \frac{n_H k_1\lambda(1-\varepsilon_{RT})(1-\varepsilon_P) - \mu\sigma_H}{k_1\sigma_H(1-\varepsilon_{RT})}.
\end{aligned}$$

E^e_{hiv} lies in the interior of the first octant if T^e_{hiv}, ${I_H}^e_{\text{hiv}}$ and ${V_H}^e_{\text{hiv}}$ are positive. It is clear that $T^e_{\text{hiv}} > 0$. Since $n_H k_1\lambda(1-\varepsilon_{RT})(1-\varepsilon_P) - \mu\sigma_H > 0$, we have ${I_H}^e_{\text{hiv}} > 0$ and ${V_H}^e_{\text{hiv}} > 0$. Hence,

$$\begin{aligned}
&n_H k_1\lambda(1-\varepsilon_{RT})(1-\varepsilon_P) - \mu\sigma_H > 0 \\
&\quad \Leftrightarrow \frac{n_H k_1\lambda(1-\varepsilon_{RT})(1-\varepsilon_P)}{\mu\sigma_H} > 1 \\
&\quad \overset{(6)}{\Leftrightarrow} \mathcal{R}_{\text{hiv}} > 1,
\end{aligned}$$

and E^e_{hiv} lies in the interior of the first octant. Now, we apply the same process as in Lemma 1 to analyze the stability of E^e_{hiv}:

Lemma 2. *If $\mathcal{R}_{\text{hiv}} > 1$, then the endemic equilibrium point E^e_{hiv} of (4) is locally asymptotically stable. Otherwise it is unstable.*

P r o o f. Let

$$\mathcal{J}^e_{\text{hiv}} = \begin{pmatrix} -\dfrac{n_H\lambda k_1(1-\varepsilon_{RT})(1-\varepsilon_P)}{\sigma_H} & 0 & -\dfrac{\sigma_H}{n_H(1-\varepsilon_P)} \\ \dfrac{n_H\lambda k_1(1-\varepsilon_{RT})(1-\varepsilon_P)-\mu\sigma_H}{\sigma_H} & -\mu & \dfrac{\sigma_H}{n_H(1-\varepsilon_P)} \\ 0 & n_H(1-\varepsilon_P)\mu & -\sigma_H \end{pmatrix}$$

be the matrix of linearization of model (4) around E^e_{hiv}. Then the associated eigenvalues are:

$$\begin{aligned}
\varphi^e_1 =& -\mu, \\
\varphi^e_2 =& -\frac{k_1\lambda n_H(1-\varepsilon_{RT})(1-\varepsilon_P)+\sigma_H^2}{2\sigma_H}, \\
&+\frac{\sqrt{n_H^2k_1^2(1-\varepsilon_{RT})^2(1-\varepsilon_P)^2\lambda^2-2n_Hk_1\sigma_H^2(1-\varepsilon_{RT})(1-\varepsilon_P)\lambda+4\mu\sigma_H^3+\sigma_H^4}}{2\sigma_H} \\
\varphi^e_3 =& -\frac{k_1\lambda n_H(1-\varepsilon_{RT})(1-\varepsilon_P)+\sigma_H^2}{2\sigma_H} \\
&-\frac{\sqrt{n_H^2k_1^2(1-\varepsilon_{RT})^2(1-\varepsilon_P)^2\lambda^2-2n_Hk_1\sigma_H^2(1-\varepsilon_{RT})(1-\varepsilon_P)\lambda+4\mu\sigma_H^3+\sigma_H^4}}{2\sigma_H}.
\end{aligned}$$

It is trivial to see that the eigenvalues φ^e_1 and φ^e_3 have negative real part. Repeating the algebraic manipulations as in Lemma 1, the eigenvalue φ^e_2 has negative real part if

$$\varphi^e_2 < 1 \Leftrightarrow \mathcal{R}_{\text{hiv}} > 1$$

and consequently, E^e_{hiv} is stable. Otherwise it is unstable. Hence, Lemma 2 is proved. □

Hence, E^e_{hiv} undergoes a transcritical bifurcation at $\mathcal{R}_{\text{hiv}} = 1$ and interchanges its stability with E_{hiv}.

We repeat the same procedure for the SARS-CoV-2 submodel as in the HIV submodel (5). Then through Theorem 2 of [21], we obtain the following lemma:

Lemma 3. *If $\mathcal{R}_{\text{sars}} < 1$, then the disease-free equilibrium point E_{sars} of (5) is locally asymptotically stable. Otherwise it is unstable.*

P r o o f. Let

$$\mathcal{J}_{\text{sars}} = \begin{pmatrix} -k_2 V_{S\text{sars}} - \mu & 0 & -k_2 T_{\text{sars}} \\ k_2 V_{S\text{sars}} & -\mu & k_2 T_{\text{sars}} \\ 0 & n_S \mu & -\sigma_S \end{pmatrix} = \begin{pmatrix} -\mu & 0 & -\dfrac{k_2 \lambda}{\mu} \\ 0 & -\mu & \dfrac{k_2 \lambda}{\mu} \\ 0 & n_S \mu & -\sigma_S \end{pmatrix} \tag{9}$$

be the matrix of linearization of model (5) around E_{sars}. Then the associated eigenvalues are:

$$\begin{aligned} \varphi_4 &= -\mu, \\ \varphi_5 &= \frac{-(\sigma_S + \mu) + \sqrt{4 n_S \lambda k_2 + (\mu - \sigma_S)^2}}{2}, \\ \varphi_6 &= \frac{-(\sigma_S + \mu) - \sqrt{4 n_S \lambda k_2 + (\mu - \sigma_S)^2}}{2}. \end{aligned}$$

Analogously to what was done in the HIV submodel, it is easy to see that the eigenvalues φ_4 and φ_6 have negative real part. Hence, if

$$\begin{aligned} -(\sigma_S + \mu) + \sqrt{4 n_S \lambda k_2 + \mu^2 - 2\mu\sigma_S + {\sigma_S}^2} < 0 \\ \Leftrightarrow 4 n_S \lambda k_2 + \mu^2 - 2\mu\sigma_S + {\sigma_S}^2 < (\sigma_S + \mu)^2 \\ \Leftrightarrow k_1 n_H (1 - \varepsilon_{RT})(1 - \varepsilon_P)\lambda < \mu\sigma_H \\ \Leftrightarrow k_2 n_S \lambda < \mu\sigma_S \\ \overset{(7)}{\Leftrightarrow} \mathcal{R}_{\text{sars}} < 1, \end{aligned}$$

then $\varphi_5 < 0$ and all eigenvalues have negative real part. This proves Lemma 3. □

Now, we compute the endemic equilibrium point for SARS-CoV-2 submodel (5). We get:

$$E^e_{\text{sars}} = (T^e_{\text{sars}}, {I_S}^e_{\text{sars}}, {V_S}^e_{\text{sars}}) = \left(\frac{\sigma_S}{n_S k_2}, \frac{n_S k_2 \lambda - \mu\sigma_S}{n_S \mu k_2}, \frac{n_S k_2 \lambda - \mu\sigma_S}{k_2 \sigma_S} \right).$$

E^e_{sars} lies in the interior of the first octant if T^e_{sars}, ${I_S}^e_{\text{sars}}$ and ${V_S}^e_{\text{sars}}$ are positive. It is clear that $T^e_{\text{sars}} > 0$. Since $n_S k_2 \lambda - \mu\sigma_S > 0$, we have ${I_S}^e_{\text{sars}} > 0$ and ${V_S}^e_{\text{sars}} > 0$. Hence,

$$\begin{aligned} n_S k_2 \lambda - \mu\sigma_S > 0 \\ \Leftrightarrow \frac{n_S k_2 \lambda}{\mu\sigma_S} > 1 \\ \overset{(7)}{\Leftrightarrow} \mathcal{R}_{\text{sars}} > 1, \end{aligned}$$

and E^e_{sars} lies in the interior of the first octant. Now, we apply the same process as in Lemma 3 to analyze the stability of E^e_{sars}:

Lemma 4. *If $\mathcal{R}_{\text{sars}} > 1$, then the endemic equilibrium point E^e_{sars} of (5) is locally asymptotically stable. Otherwise it is unstable.*

P r o o f. Let

$$\mathcal{J}^e_{\text{sars}} = \begin{pmatrix} -\dfrac{n_H \lambda k_2}{\sigma_S} & 0 & -\dfrac{\sigma_S}{n_S} \\ \dfrac{n_H \lambda k_2 - \mu\sigma_S}{\sigma_S} & -\mu & \dfrac{\sigma_S}{n_S} \\ 0 & n_S\mu & -\sigma_S \end{pmatrix}$$

be the matrix of linearization of model (5) around E^e_{sars}. Then the associated eigenvalues are:

$$\begin{aligned} \varphi^e_4 &= -\mu, \\ \varphi^e_5 &= -\frac{k_2\lambda n_S + \sigma_S^2 - \sqrt{n_S^2 k_2^2 \lambda^2 - 2n_S k_2 \sigma_S^2 \lambda + 4\mu\sigma_S^3 + \sigma_S^4}}{2\sigma_S}, \\ \varphi^e_6 &= -\frac{k_2\lambda n_S + \sigma_S^2 + \sqrt{n_S^2 k_2^2 \lambda^2 - 2n_S k_2 \sigma_S^2 \lambda + 4\mu\sigma_S^3 + \sigma_S^4}}{2\sigma_S}. \end{aligned}$$

It is trivial to see that the eigenvalues φ^e_4 and φ^e_6 have negative real part. Repeating the algebraic manipulations as in Lemma 1, the eigenvalue φ^e_5 has negative real part if

$$\varphi^e_5 < 1 \Leftrightarrow \mathcal{R}_{\text{sars}} > 1$$

and consequently, E^e_{sars} is stable. Otherwise it is unstable. Hence, Lemma 4 is proved. □

6. Proof of Theorem 3

We analyze the full model (1). The disease-free equilibrium point of system (1) is given by

$$E_{\text{DFE}} = (T^\star, {I_H}^\star, {I_S}^\star, {V_H}^\star, {V_S}^\star, C^\star) = \left(\frac{\lambda}{\mu}, 0, 0, 0, 0, 0\right).$$

The proof of the first result of this theorem follows from the result obtained by the authors of [21], i.e., the basic reproduction number of a model with multiples infections in interaction can be approximated as the maximum of the basic reproduction number of each submodel. This result is valid because, in the long-term dynamics of the system, the infection with the highest basic reproduction number controls the

spread of the disease, which determines whether or not the infection can persist in the population. Accordingly, applying this principle to (1), the basic reproduction number is given by

$$\mathcal{R}_0 = \max\{\mathcal{R}_{\text{hiv}}, \mathcal{R}_{\text{sars}}\}.$$

Now, let

$$\mathcal{J}_{\text{f}} = \begin{pmatrix} -k_1(1-\varepsilon_{RT})V_H^\star - k_2 V_S^\star - \mu & 0 & 0 & -k_1(1-\varepsilon_{RT})T^\star & -k_2 T^\star & 0 \\ k_1(1-\varepsilon_{RT})V_H^\star & -(k_2 V_S^\star + \mu) & 0 & k_1(1-\varepsilon_{RT})T^\star & -k_2 I_H^\star & 0 \\ k_2 V_S^\star & 0 & -(k_1(1-\varepsilon_{RT})V_H^\star + \mu) & -k_1(1-\varepsilon_{RT})I_S^\star & k_2 T^\star & 0 \\ 0 & n_H\mu(1-\varepsilon_P) & 0 & -\sigma_H & 0 & 0 \\ 0 & 0 & n_S\mu & 0 & -\sigma_S & 0 \\ 0 & k_2 V_S^\star & k_1(1-\varepsilon_{RT})V_H^\star & -k_1(1-\varepsilon_{RT})I_S^\star & k_2 I_H^\star & -\mu \end{pmatrix}$$

$$= \begin{pmatrix} -\mu & 0 & 0 & -k_1(1-\varepsilon_{RT})\lambda/\mu & -k_2\lambda/\mu & 0 \\ 0 & -\mu & 0 & k_1(1-\varepsilon_{RT})\lambda/\mu & 0 & 0 \\ 0 & 0 & -\mu & 0 & k_2\lambda/\mu & 0 \\ 0 & n_H(1-\varepsilon_P)\mu & 0 & -\sigma_H & 0 & 0 \\ 0 & 0 & n_S\mu & 0 & -\sigma_S & 0 \\ 0 & 0 & 0 & 0 & 0 & -\mu \end{pmatrix}$$

be the matrix of linearization of (1) around E_{DFE}. Then the associated eigenvalues are

$$\varphi_1,\ \varphi_2,\ \varphi_3,\ \varphi_4,\ \varphi_5 \quad \text{and} \quad \varphi_6,$$

the same eigenvalues of (8) and (9) combined. We already know that φ_1, φ_3, φ_4 and φ_6 have negative real part and φ_2 and φ_5 have negative real part if $\mathcal{R}_{\text{hiv}}$ and $\mathcal{R}_{\text{sars}}$ are less than one. Therefore, E_{DFE} is asymptotically stable if $\mathcal{R}_0 < 1$ and Theorem 3 is proved.

7. Numerics

In this section, we present several numerical simulations to analyze the dynamics of HIV and SARS-CoV-2 coinfection. By varying the efficacy of ε_{RT} and ε_P, we explore how these treatments impact infected cells and viral loads over time. We use the parameter values given in Table 2 for all figures.

Figure 2 shows the dynamics of HIV-infected cells I_H and HIV viral load V_H of (4) for different values of ε_{RT} and ε_P, representing the effectiveness of RTI and PI. A noticeable decline in both I_H and V_H populations is observed over time for all cases, with a more rapid and effective reduction as the treatment efficacy parameters increase. We also observe that when treatment efficacy is high enough, the number of HIV-infected cells is higher than the HIV viral load. Figure 3 illustrates the dynamics of I_S and V_S over time, for the submodel (5). The dashed curve, representing I_S, increases rapidly until it stabilizes, while the continuous curve, representing V_S, remains practically constant and much lower than I_S. However, it can be seen

Parameter	Symbol	Value	Reference
Constant production rate of T cells	λ	10 cells mm^{-3}	[1]
HIV infection rate	k_1	10^{-8} virions mm^3 day^{-1}	[11]
SARS-CoV-2 infection rate	k_2	10^{-3} virions mm^3 day^{-1}	[20]
RTI-based treatment efficacy	ε_{RT}	[0,1]	—
PI drug efficacy	ε_P	[0,1]	—
Bursting size for HIV growth	n_H	$42 - 88$ virions cell^{-1}	[18]
Bursting size for SARS-CoV-2 growth	n_S	$10 - 2500$ virions cell^{-1}	[1]
Natural death rate of T, I_H, I_S and C cells	μ	10^{-2} day^{-1}	[1]
Death rate of HIV	σ_H	$2 - 3$ day^{-1}	[18]
Death rate of SARS-CoV-2	σ_S	3 day^{-1}	[1]

Table 2. Parameter values used in numerical simulations.

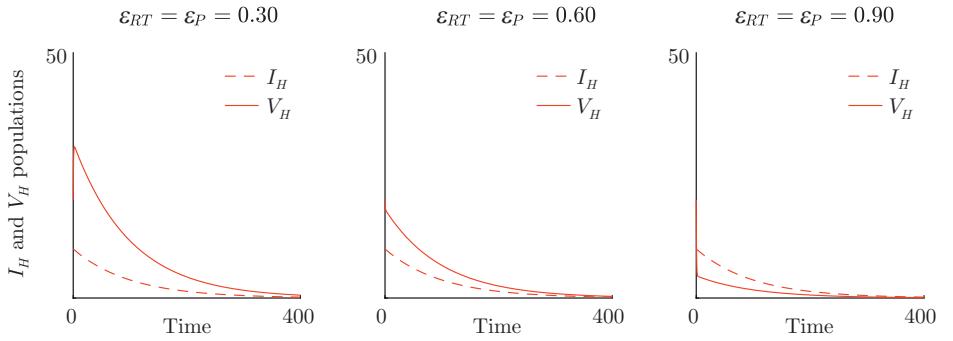

Figure 2. I_H and V_H dynamics of system (4) for different values of ε_{RT} and ε_P. Initial conditions: $(T, I_H, V_H) = (10, 10, 20)$.

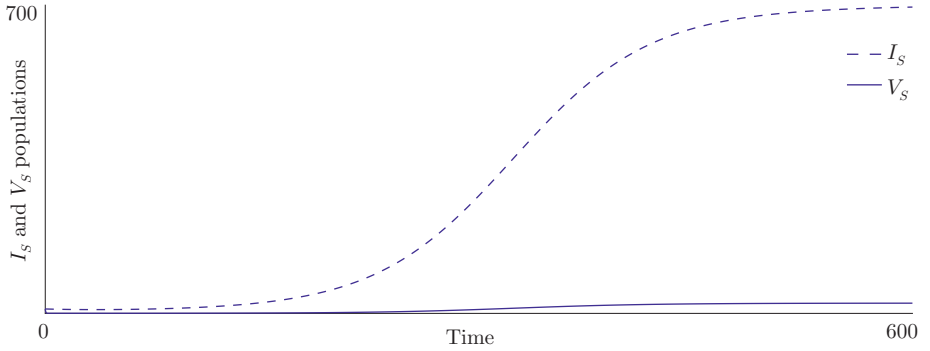

Figure 3. I_S and V_S dynamics of system (5). Initial conditions: $(T, I_S, V_S) = (10, 10, 10)$.

that at the inflection point of the curve of I_S, there is also a slight increase in viral concentration, so this seems to be a coherent conclusion and in line with the simulation observation. Figure 4 shows the dynamics of I_H, I_S and coinfected cells with both viruses C over time, for different treatment efficacy values ε_{RT} and ε_P:

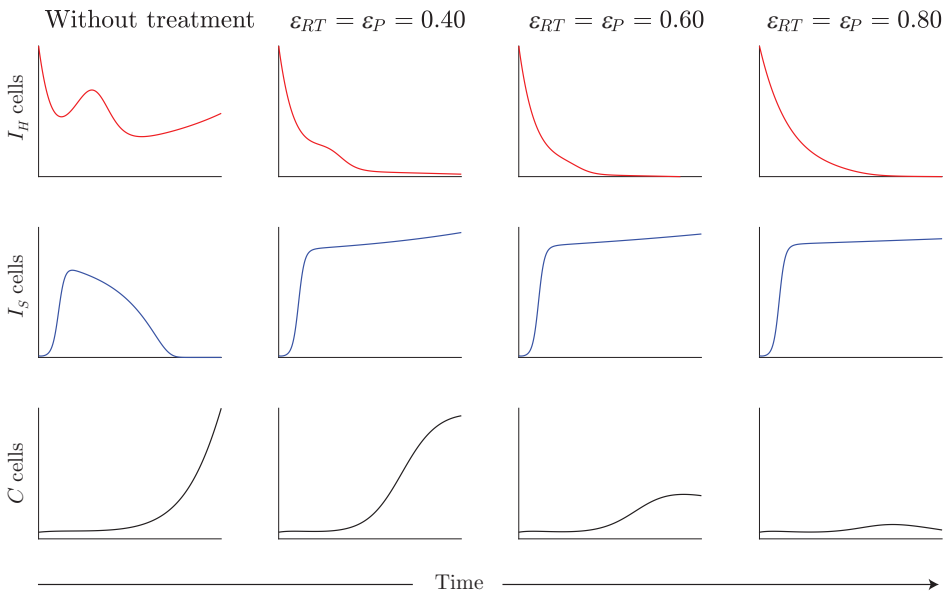

Figure 4. I_H, I_S and C dynamics of system (1) for different values of ε_{RT} and ε_P. Initial conditions: $(T, I_H, I_S, V_H, V_S, C) = (10, 60, 10, 50, 1, 1)$.

- ▷ In the first column "without treatment", the number of HIV-infected cells shows an oscillatory behavior before decreasing. Initially, the number of cells infected with SARS-CoV-2 increases significantly. Asymptotically, the number of these cells tends to zero. The number of coinfected cells increases exponentially;
- ▷ With increasing treatment efficacy $\varepsilon_{RT} = \varepsilon_P$ from 40% to 80%, a faster decrease in I_H cells is observed. I_S cells continue to grow, but the growth rate decreases as treatment efficacy increases. The number of coinfected cells tends to decrease as the effectiveness of the treatments increases.

Figure 5 shows the dynamics of V_H and V_S over time, for different values of ε_{RT} and ε_P:

- ▷ In the first column, "Without treatment", the HIV viral load increases in an approximately linear fashion. On the other hand, the concentration of SARS-CoV-2 increases quickly, reaches a peak and then decreases until it stabilizes near zero;
- ▷ As treatment efficacy, $\varepsilon_{RT} = \varepsilon_P$, increases from 40% to 80%, two scenarios occur: (i) V_H begins to be controlled more efficiently, leading to a decrease in the viral load; (ii) For any value of the effectiveness of the treatment, V_S has a similar asymptotic behavior, increasing rapidly at first and then stabilizing this rate of increase. However, this growth is reduced as ε_{RT} and ε_P increase.

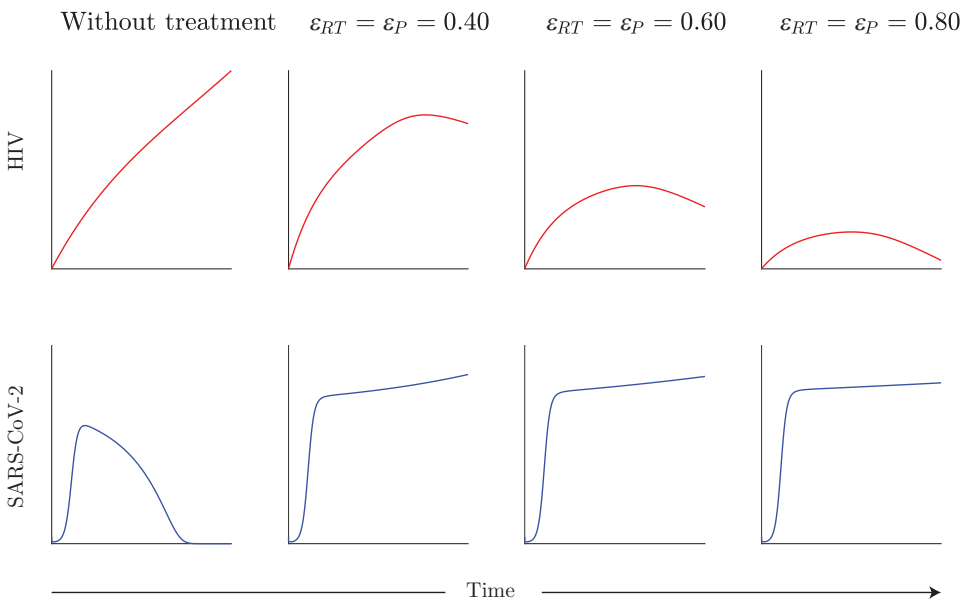

Figure 5. V_H and V_S dynamics of system (1) for different values of ε_{RT} and ε_P. Initial conditions: $(T, I_H, I_S, V_H, V_S, C) = (10, 60, 10, 50, 1, 1)$.

The simulation in Figure 6 shows that antiretroviral therapy has an influence on the dynamics of SARS-CoV-2 infected cells when in an environment where there are also HIV-infected cells. It reveals that the higher the ε_{RT} and the lower the ε_P, the slower the growth of I_S and V_S, even though both grow continuously.

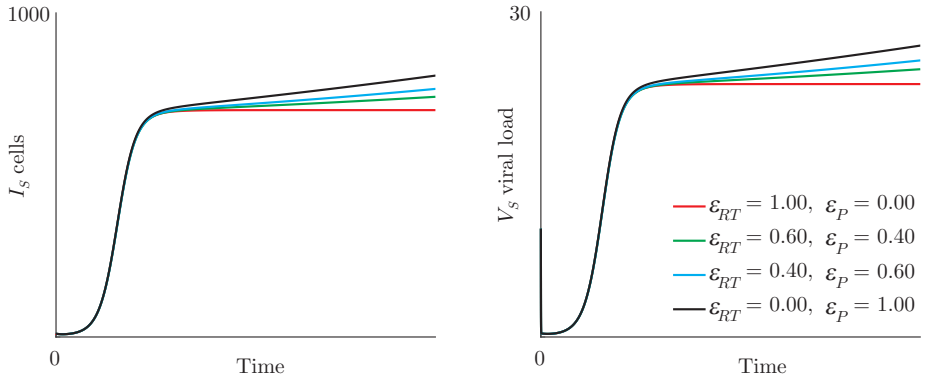

Figure 6. I_S and V_S dynamics of system (1) and under HAART therapy with parameter combination $\varepsilon_{RT} + \varepsilon_P = 1$. Initial conditions: $(T, I_H, I_S, V_H, V_S, C) = (10, 10, 10, 10, 10, 1)$.

8. Conclusions

In this work we have analyzed a mathematical model to understand the dynamics of infection of healthy T cells by HIV and SARS-CoV-2 under the effect of HAART. We have shown that the solutions of model (1) are positive and bounded within a biologically reasonable region (Theorem 1). Furthermore, we have computed the disease-free and endemic equilibria for HIV and SARS-CoV-2 submodels and their respective basic reproduction numbers, $\mathcal{R}_{\text{hiv}}$ and $\mathcal{R}_{\text{sars}}$. We have proved that the endemic equilibria of each submodel undergo a transcritical bifurcation when the respective basic reproduction number equals one (Theorem 2). Hence, for submodels (4) and (5), we have shown that the disease-free equilibria are stable when the respective basic reproduction number is less than 1 and unstable otherwise. Their endemic equilibria are stable when the basic reproduction number is greater than one and unstable otherwise. Finally, regarding system (1), we have shown that the basic reproduction number for the coinfection model is expressed as $\mathcal{R}_0 = \max\{\mathcal{R}_{\text{hiv}}, \mathcal{R}_{\text{sars}}\}$, and that the disease-free equilibrium point remains stable when $\mathcal{R}_0 < 1$ (Theorem 3).

Lastly, regarding the numerical results, we have concluded that antiretroviral therapy has a significant impact in reducing both HIV viral load and HIV-infected cells (Figure 2). Moreover, although HAART specifically targets HIV and HIV-infected cells, Figures 4, 5 and 6 have indicated that this therapy also reduces SARS-CoV-2 proliferation and SARS-CoV-2-infected cells. Consequently, HAART has proven highly effective in reducing coinfected cells, with greater reductions observed as the efficacy of HAART improves (Figure 4). These findings suggest that HAART, while primarily targeting HIV, may also reduce SARS-CoV-2 proliferation in coinfected individuals, likely due to enhanced immune function and fewer susceptible cells. This highlights a potential added benefit of HAART in coinfection scenarios and may inform clinical management.

Model validation and future work. This study presents a theoretical mathematical model designed to understand the interaction between HIV and SARS-CoV-2 infections under HAART. The main focus is on the qualitative behaviour of the model, including the analysis of bifurcations and the stability of equilibria. The model has not been calibrated with real-world biological data, as such validation is beyond the scope of this work. However, we recognise the importance of assessing the model's reliability in real-world scenarios. A future research direction would be to incorporate data fitting procedures, such as parameter estimation using least squares methods or Bayesian inference, and to validate the model's predictions against available clinical datasets of coinfected patients. These extensions would increase the applicability of the model and could provide more information on the biological relevance of the theoretical results. Moreover, we plan to extend our current coinfection

model to examine the effects of SARS-CoV-2 vaccination on HIV progression. While this study focused on the influence of HAART on SARS-CoV-2 dynamics, the new approach will assess how COVID-19 vaccines [16] can impact HIV viral load and the number of HIV-infected cells.

Data and code availability. All code and scripts used to generate the results presented in this manuscript are openly available at: `https://doi.org/10.5281/zenodo.15519037`. No data was used for the research described in the article.

References

[1] *N. Bairagi, D. Adak*: Dynamics of cytotoxic T-lymphocytes and helper cells in human immunodeficiency virus infection with Hill-type infection rate and sigmoidal CTL expansion. Chaos Solitons Fractals *103* (2017), 52–67. zbl MR doi

[2] *K. T. Bajgain, S. Badal, B. B. Bajgain, M. J. Santana*: Prevalence of comorbidities among individuals with COVID-19: A rapid review of current literature. Am. J. Infect. Control *49* (2021), 238–246. doi

[3] *D. Basoulis, E. Mastrogianni, P.-M. Voutsinas, M. Psichogiou*: HIV and COVID-19 co-infection: Epidemiology, clinical characteristics, and treatment. Viruses *15* (2023), Article ID 577, 21 pages. doi

[4] *T. D. Batu, L. L. Obsu, C. T. Deressa*: Co-infection dynamics of COVID-19 and HIV/AIDS. Sci. Report. *13* (2023), Article ID 18437, 21 pages. doi

[5] *F. Brauer, C. Castillo-Chavez*: Mathematical Models in Population Biology and Epidemiology. Texts in Applied Mathematics 40. Springer, New York, 2012. zbl MR doi

[6] *W. Chen, L. Zhang, N. Wang, Z. Teng*: Bifurcation analysis and chaos for a double-strains HIV coinfection model with intracellular delays, saturated incidence and logistic growth. Math. Comput. Simul. *223* (2024), 617–641. zbl MR doi

[7] *N. Chitnis, J. M. Hyman, J. M. Cushing*: Determining important parameters in the spread of malaria through the sensitivity analysis of a mathematical model. Bull. Math. Biol. *70* (2008), 1272–1296. zbl MR doi

[8] *M. A. Höft, W. A. Burgers, C. Riou*: The immune response to SARS-CoV-2 in people with HIV. Cell. Mol. Immunol. *21* (2024), 184–196. doi

[9] *B. Hu, H. Guo, P. Zhou, Z.-L. Shi*: Characteristics of SARS-CoV-2 and COVID-19. Nat. Rev. Microbiol. *19* (2021), 141–154. doi

[10] *J. P. S. Maurício de Carvalho, B. Moreira-Pinto*: A fractional-order model for CoViD-19 dynamics with reinfection and the importance of quarantine. Chaos Solitons Fractals *151* (2021), Article ID 111275, 7 pages. MR doi

[11] *J. P. S. Maurício de Carvalho, C. M. A. Pinto*: Role of the immune system in AIDS-defining malignancies. Perspectives in Dynamical Systems I. Mechatronics and Life Sciences. Springer Proceedings in Mathematics & Statistics 362. Springer, Cham, 2022, pp. 95–105. zbl doi

[12] *K. G. Mekonena, L. L. Obsu*: Mathematical modeling and analysis for the co-infection of COVID-19 and tuberculosis. Heliyon *8* (2022), Article ID e11195, 11 pages. doi

[13] *D. Moriconi, S. Masi, E. Rebelos, A. Virdis, M. L. Manca, S. De Marco, S. Taddei, M. Nannipieri*: Obesity prolongs the hospital stay in patients affected by COVID-19, and may impact on SARS-COV-2 shedding. Obesity Research Clin. Pract. *14* (2020), 205–209. doi

[14] *R. Musa, O. J. Peter, F. A. Oguntolu*: A non-linear differential equation model of COVID-19 and seasonal influenza co-infection dynamics under vaccination strategy and immunity waning. Healthcare Anal. *4* (2023), Article ID 100240, 20 pages. doi

[15] *O. J. Peter, C. E. Madubueze, M. M. Ojo, F. A. Oguntolu, T. A. Ayoola*: Modeling and optimal control of monkeypox with cost-effective strategies. Model. Earth Syst. Environ. *9* (2023), 1989–2007. doi

[16] *O. J. Peter, H. S. Panigoro, A. Abidemi, M. M. Ojo, F. A. Oguntolu*: Mathematical model of COVID-19 pandemic with double dose vaccination. Acta Biotheor. *71* (2023), Article ID 9, 30 pages. doi

[17] *H. A. Rothan, S. N. Byrareddy*: The epidemiology and pathogenesis of coronavirus disease (COVID-19) outbreak. J. Autoimmun. *109* (2020), Article ID 102433, 4 pages. doi

[18] *P. K. Roy, N. Bairagi, J. Chattopadhyay, B. Chattopadhyay*: HIV model with intracellular delay – A mathematical study. IEEE International Conference on Automation Science and Engineering 2009. IEEE, Los Alamitos, 2009, pp. 373–378. doi

[19] *J. Sun, W.-T. He, L. Wang, A. Lai, X. Ji, X. Zhai, G. Li, M. A. Suchard, J. Tian, J. Zhou, M. Veit, S. Su*: COVID-19: Epidemiology, evolution, and cross-disciplinary perspectives. Trends Molecul. Med. *26* (2020), 483–495. doi

[20] *S. Tang, W. Ma, P. Bai*: A novel dynamic model describing the spread of the MERS-CoV and the expression of dipeptidyl peptidase 4. Comput. Math. Methods Med. *2017* (2017), Article ID 5285810, 6 pages. zbl MR doi

[21] *P. van den Driessche, J. Watmough*: Reproduction numbers and sub-threshold endemic equilibria for compartmental models of disease transmission. Math. Biosci. *180* (2002), 29–48. zbl MR doi

[22] *B. Vemparala, S. Chowdhury, J. Guedj, N. M. Dixit*: Modelling HIV-1 control and remission. npj Syst. Biol. Appl. *10* (2024), Article ID 84, 11 pages. doi

[23] *A. Vitiello, F. Ferrara, C. Pelliccia, G. Granata, R. La Porta*: Cytokine storm and colchicine potential role in fighting SARS-CoV-2 pneumonia. Ital. J. Med. *14* (2020), 88–94. doi

[24] *World Health Organization (WHO)*: COVID-19 Cases, World. Available at `https://covid19.who.int` (Accessed 30 April 2025).

[25] *World Health Organization (WHO)*: HIV and AIDS. Available at `https://www.who.int/news-room/fact-sheets/detail/hiv-aids` (Accessed 30 April 2025).

Author's addresses: *João Paulo Simões Maurício de Carvalho*, Centre for Mathematics, University of Porto, Rua do Campo Alegre s/n, Porto 4169-007, Portugal; Prince Henry Portucalense University, Rua Dr. António Bernardino de Almeida 541, Porto 4200-072, Portugal, e-mail: `jp.carvalho@upt.pt`.